


cambridge.org/mrf

Fatima Ez-Zaki<sup>1</sup> , Hassan Belahrach<sup>1,2</sup> and Abdelilah Ghammaz<sup>1</sup>

<sup>1</sup>Laboratory of Electrical Systems and Telecommunications, Faculty of Sciences and Technologies, Cadi Ayyad University, Marrakesh, Morocco and <sup>2</sup>Royal School of Aeronautics, Marrakesh, Morocco

## Research Paper

**Cite this article:** Ez-Zaki F, Belahrach H, Ghammaz A (2021). Broadband microstrip antennas with Cantor set fractal slots for vehicular communications. *International Journal of Microwave and Wireless Technologies* **13**, 295–308. <https://doi.org/10.1017/S1759078720000719>

Received: 24 January 2020  
Revised: 4 May 2020  
Accepted: 6 May 2020  
First published online: 8 June 2020

### Keywords:

Cantor set fractal; hexagonal microstrip patch antenna; vehicular communications

### Author for correspondence:

Fatima Ez-Zaki,  
E-mail: [ftimaezzaki@gmail.com](mailto:ftimaezzaki@gmail.com)

## Abstract

Vehicle-to-everything communications (V2X), whose main objective is to improve security and efficiency, are provided by ad hoc vehicle networks that allow communication between vehicles. In the current study, a hexagonal microstrip patch antenna has been developed to cover the navigational frequencies, WiMAX at 3.7 GHz and DSRC/IEEE802.11p at 5.9 GHz to meet the demands of various vehicular applications. The antenna design is based on Cantor fractal slot, partial ground plane, and inset feed which is directly fed through the microstrip line. The proposed antenna shields the frequency band from 3.22 to 6.5 GHz with VSWR <2 within all the frequency bands. The presented antenna can resonate well in the 5.85–5.95 GHz band assigned for DSRC/IEEE802.11p and 3.7 GHz assigned for LTE/V2X. Simulated antenna gain varies from 3.06 to 5.25 dB within the operated frequency range providing an omnidirectional simulated radiation pattern in the most azimuth plane. To prove the validity of the simulation results, the chosen antenna structure has been fabricated and tested using a vector network analyzer MS2630. The measurement shows good results, which make the antenna suitable for wireless applications of interest.

## Introduction

Recently, owing to the progress of communication services and transport systems, major technical innovations have marked, by their importance, the growth of telecommunication. However, a new decentralized architecture based on vehicular communications has aroused real interest of telecommunication industries, research communities, and the automotive industry [1].

To reduce traffic congestion, improve road safety, and increase traffic efficiency, modern vehicles can contain several antennas for different wireless applications such as AM/FM radio, remote keyless entry, satellite navigation, digital satellite radio, and vehicle-to-everything (V2X) communications [2]. In addition to existing applications, vehicular communications will be covered by technologies such as DSRC/IEEE 802.11p and cellular technology/LTE [3–6]. The reliability and the efficiency of these technologies depend mostly on the quality of the communication link, where antennas are one among the critical modules [2,7]. Indeed, finding optimal antenna performance is incredibly crucial. Besides, due to the high number of antennas and the limited space on the vehicle, the development and use of multi-band antennas is needed [2, 6, 7].

Microstrip patch antennas (MPA) have many advantages in communication systems; their thickness, low cost, compact size, and easy integration into peripherals makes them appropriate for this kind of communication [2]. But the associated MPAs have disadvantages such as low gain, narrow bandwidth, and lower efficiency [8, 9]. To surmount these drawbacks and with the increasing demand of multiband antennas, fractal geometry is a good option. Fractal antennas present two benefits [10, 11]. First, these antennas have a geometric specificity that allows them to resonate over several frequencies while possibly keeping the same electromagnetic characteristics, which is known by the self-similarity or similarity of geometric shape at different scales. Second, the space-filling efficiency of some fractal shapes gives hope for smaller antennas compared to the conventional ones. These benefits make them simpler and easier to manufacture multiband and wideband antennas. The application of this type of vehicular antennas has been studied by several researchers [2, 3, 5, 6, 12]. Therefore, much research has been conducted on designing antennas capable of covering different bands of frequencies [7, 12–14]. The authors in [3–6, 15] have focused on the design and performance of LTE and DSRC antennas. The studies conferred in [13–22] projected modules of IEEE 802.11p/DSRC antennas. A compact antenna for V2X communication based on LTE and IEEE 802.11p technologies has presented in [3]. The study in [5] presents a new antenna model appropriate to V2V communications based on LTE and the IEEE 802.11 standard. Considering the disadvantages of existing V2V communication antennas, the authors in [18] offer a regular broadband antenna with a relative bandwidth of 35.55%.

**Table 1.** IFS transformation coefficient for Cantor set fractal

$w_i$	$a_i$	$b_i$	$c_i$	$d_i$	$e_i$	$f_i$
1	0.3	0	0	1	0	0
2	0.3	0	0	1	0.6	0

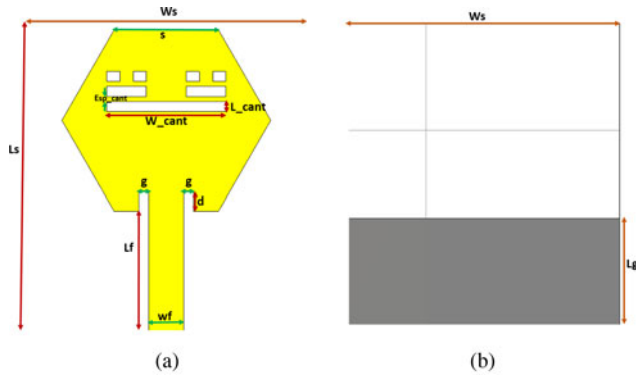


**Fig. 1.** The proposed antenna configuration: (a) front view and (b) back view.

This study elaborates on the design of a hexagonal microstrip patch antenna (HMPA) of a compact size of  $31 \times 28 \times 1.6 \text{ mm}^3$ . The projected antenna illustrates a wider bandwidth (from 3.2 to 6.5 GHz) by the combination of Cantor fractal slots introduced on the patch and partial ground plane below. Mathematical modeling of the investigated HMPA and the antenna geometry design

followed by a parametric study of critical geometrical variables are described in Section “Antenna design and parametric study.” While Section “Results and discussion” presents the discussion of the simulated and measurement results of the proposed antenna in terms of  $S_{11}$  parameter, VSWR, bandwidth, gain, current distribution, and radiation patterns. Section “Antenna positioning on the vehicle” depicts the various antenna positioning on the vehicle. Finally, conclusion of the study is given.

### Antenna design and parametric study

This section presents the mathematical modeling of an HMPA and simulated results given by a simple parametric study.

#### Antenna design

Using the cavity model, the resonant frequencies of the TM mode of a circular patch are given in equation (1) [23]:

$$f_r = \frac{cX_{np}}{2\pi a_{eff} \sqrt{\epsilon_r}}, \tag{1}$$

where  $c$  is the light velocity in the free space,  $\epsilon_r$  is the relative permittivity of the substrate, and  $X_{np}$  are the zeros of the derivative of the Bessel function  $J_n(x)$  of order  $n$ , as is true of TE-mode circular waveguides. The lowest-order mode,  $TM_{11}$ , uses  $X_{11} = 1.84118$  and produces a linearly polarized field similar to a square patch.  $a_{eff}$  is an effective radius of the patch taking fringing into account. As is known, the fringing gives a wider electrical aspect to the patch, and it has been taken into account by introducing a correction factor. For the circular patch, a correction is introduced

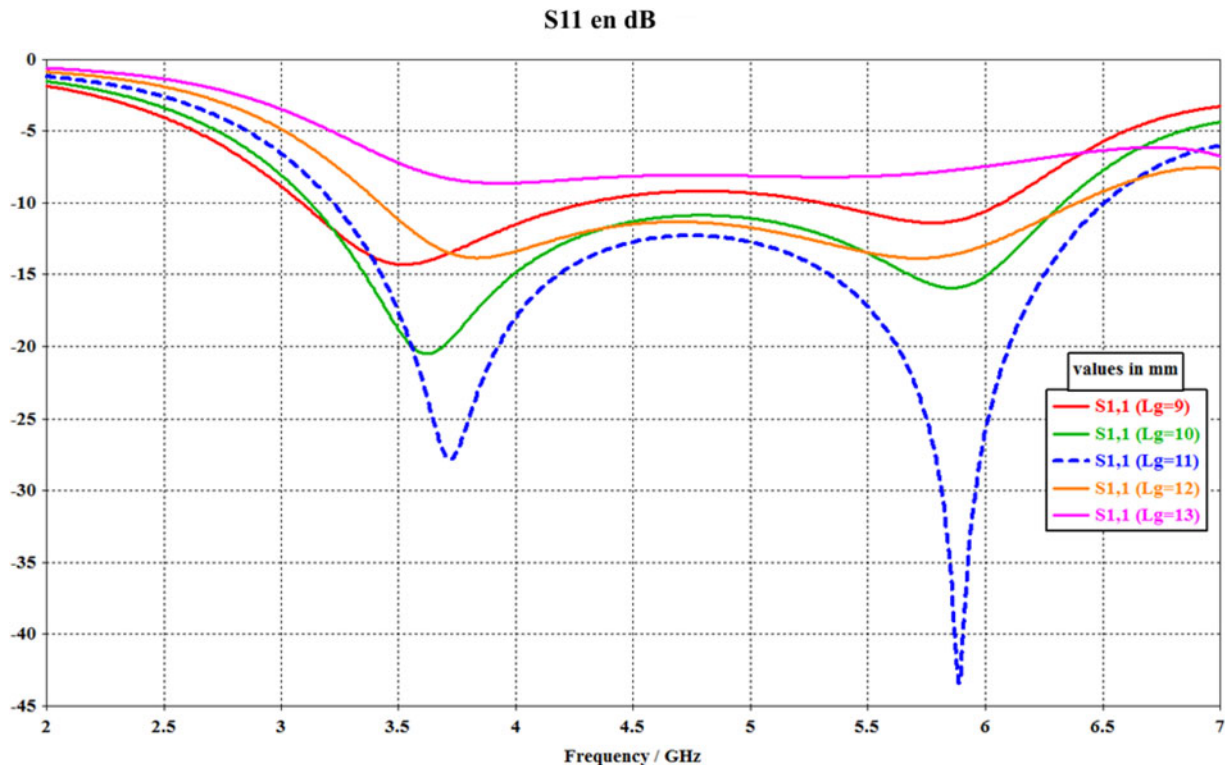


**Fig. 2.** Effect of various lengths of the ground plane ( $L_g$ ) on  $S_{11}$ .

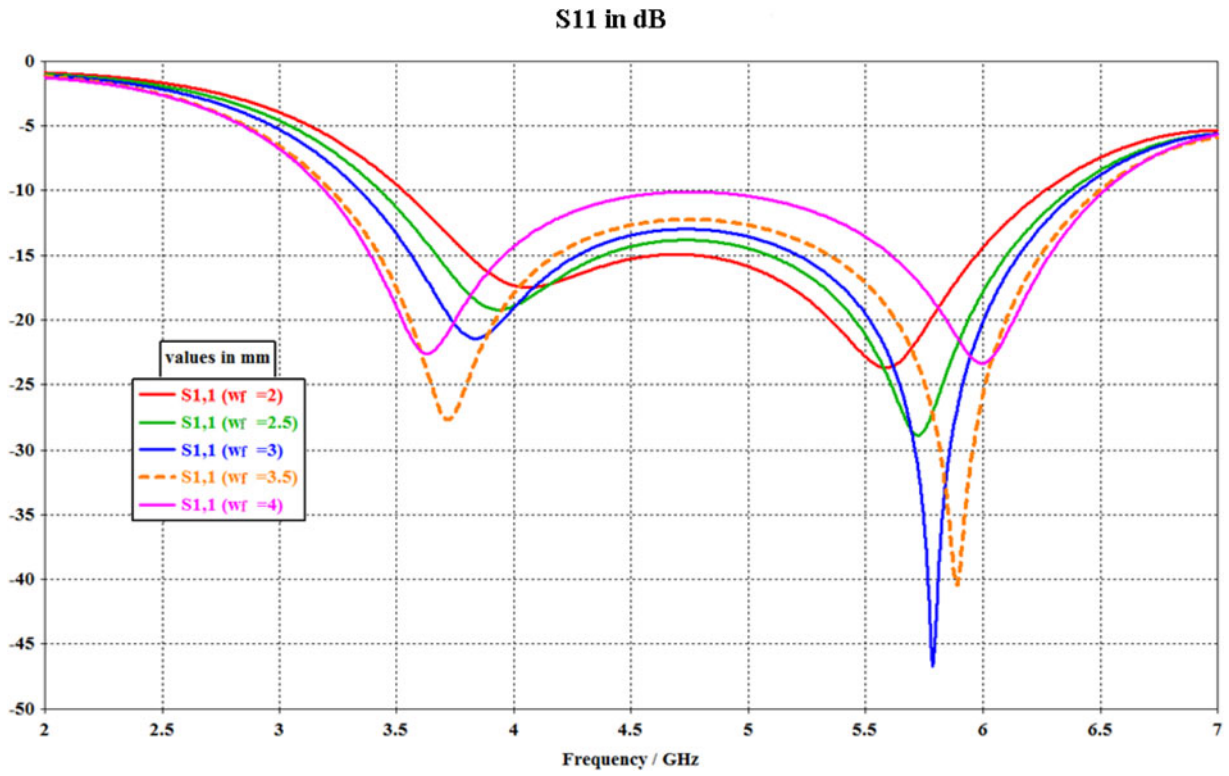


Fig. 3. Effect of various widths of the feed line ( $wf$ ) on  $S_{11}$ .

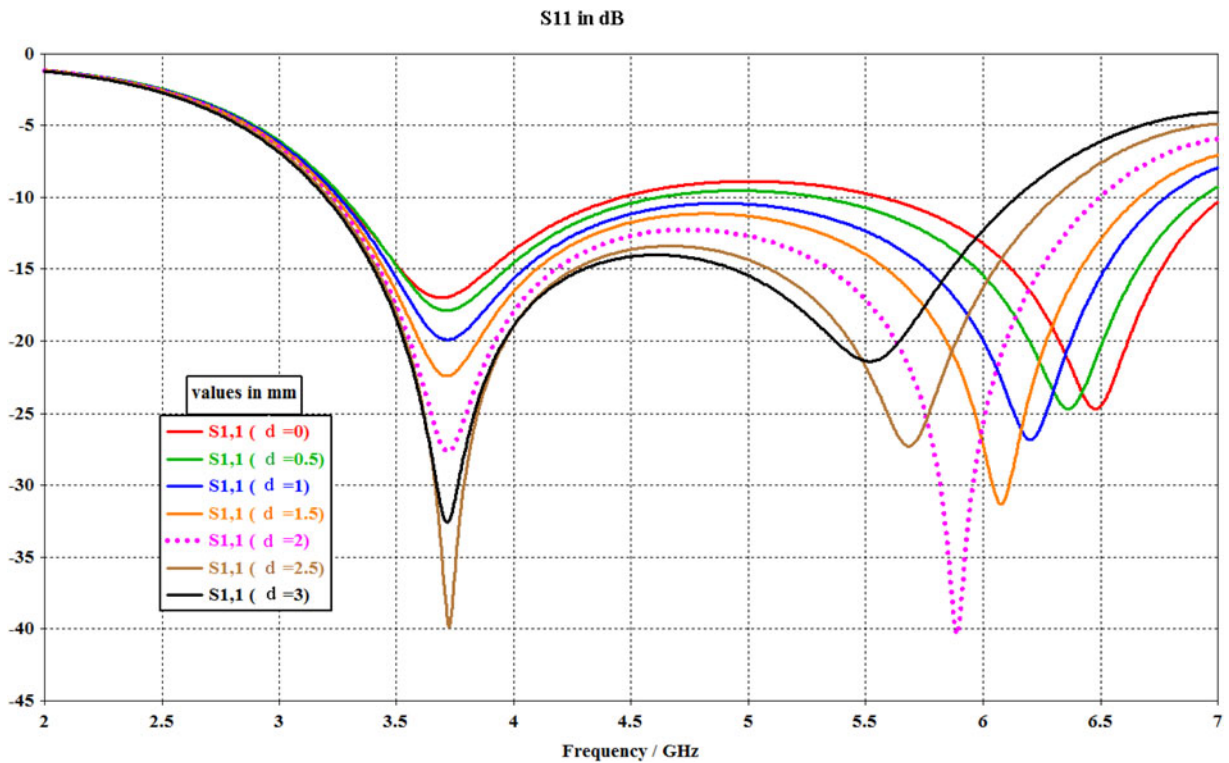


Fig. 4.  $S_{11}$  for various inset feed line distances ( $d$ ).

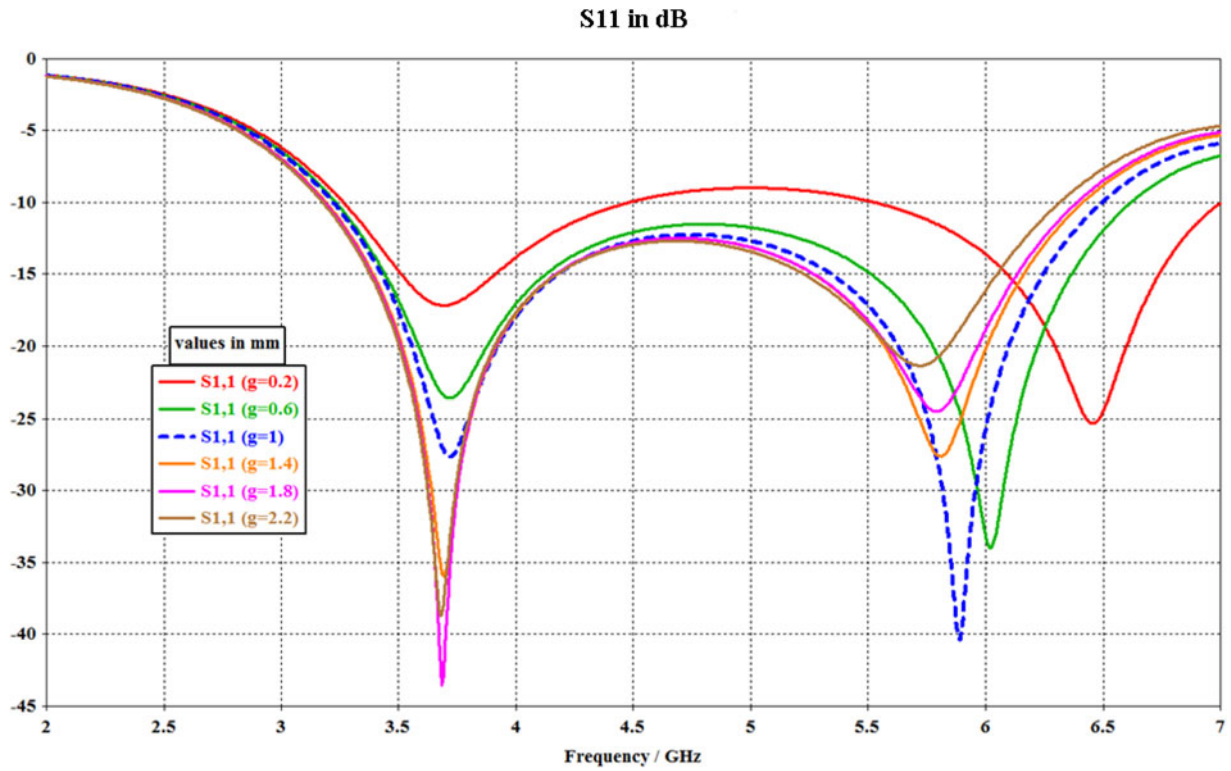


Fig. 5.  $S_{11}$  for various gaps ( $g$ ).

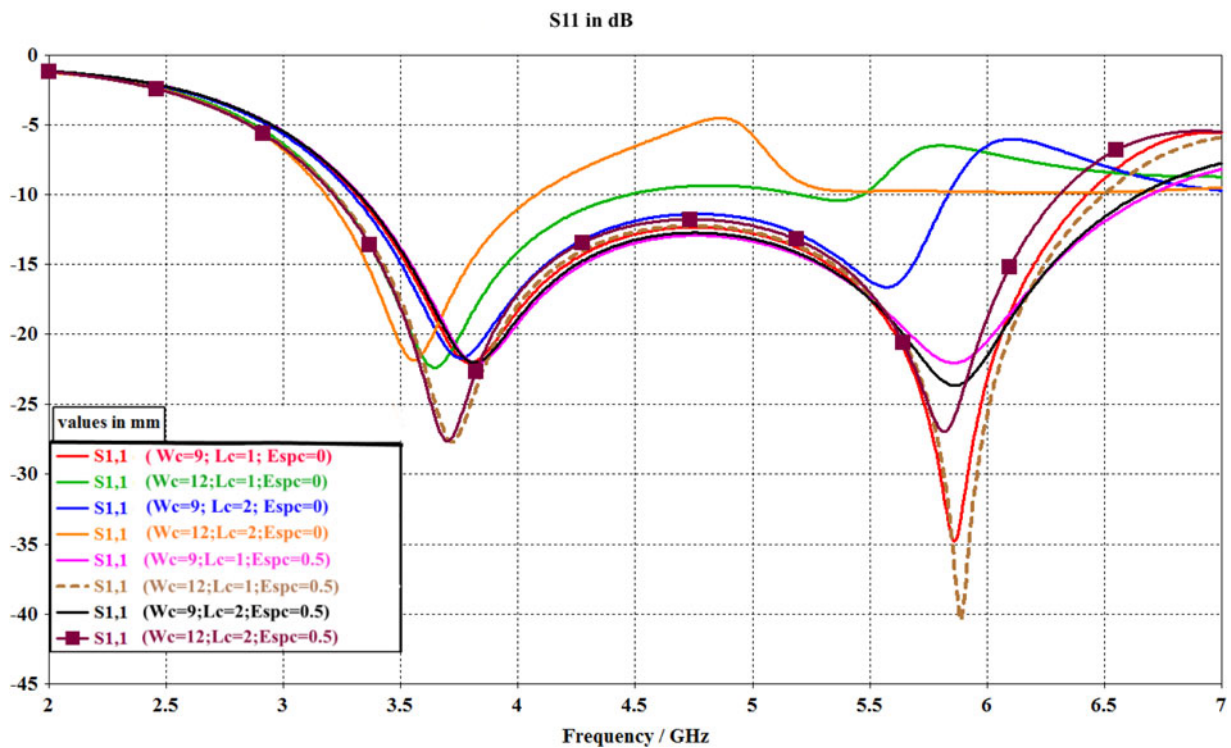


Fig. 6.  $S_{11}$  for various Cantor set dimensions values.

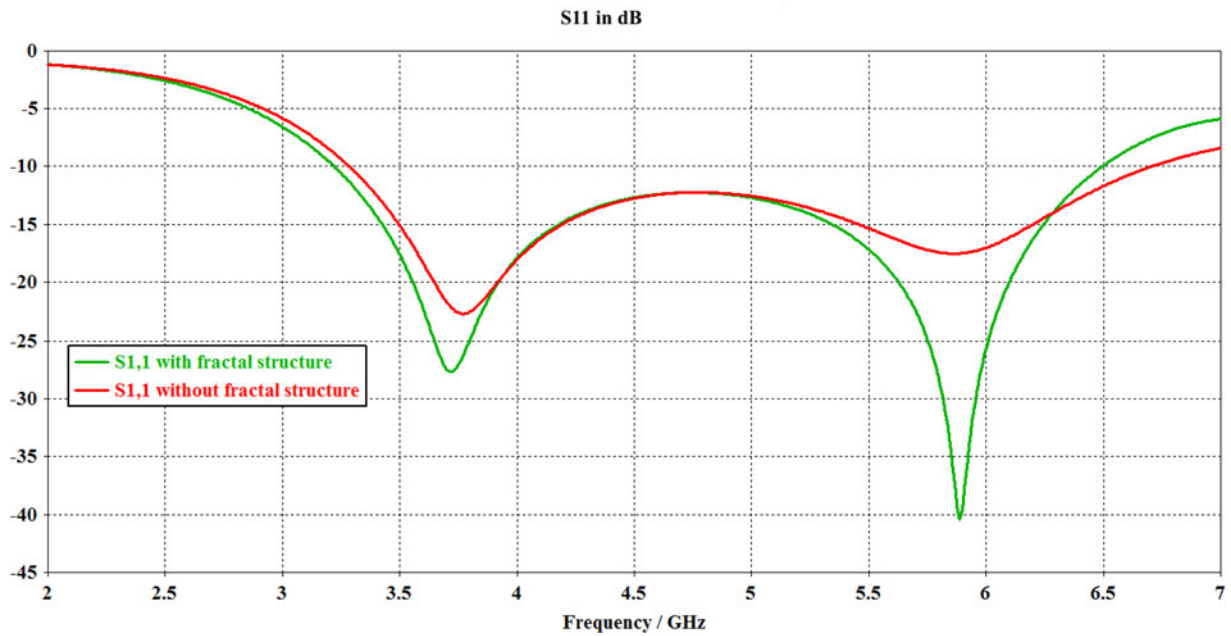


Fig. 7. Return loss comparison of both configurations.

Table 2. The optimal dimensions of the proposed antenna

Antenna parameters	Values (mm)
<i>Ls</i>	31
<i>Ws</i>	28
<i>Lg</i>	11
<i>h</i>	1.6
<i>wf</i>	3.5
<i>Lf</i>	12
<i>d</i>	2
<i>g</i>	1
<i>s</i>	10.5
<i>Lc</i>	12
<i>Wc</i>	1
<i>Espc</i>	0.5

using an effective radius  $a_{eff}$ , to replace the real radius  $a$ , given in [23]:

$$a_{eff} = a \left\{ 1 + \frac{2h}{\pi\epsilon_r a} \left( \ln\left(\frac{\pi a}{2h}\right) + 1.7726 \right) \right\}^{1/2}, \quad (2)$$

where  $h$  is the height of the substrate. Since the effective and physical radii of the patch are nearly the same, equation (2) may be iterated to compute the real radius  $a$  given by equation (3):

$$a = \frac{F}{\left\{ 1 + \frac{2h}{\pi\epsilon_r F} \left( \ln\left(\frac{\pi F}{2h}\right) + 1.7726 \right) \right\}^{1/2}} \quad (3)$$

where  $h$  is in cm, and

$$F = \frac{8.791 \times 10^9}{f_r \sqrt{\epsilon_r}} \quad (4)$$

By relating the areas of the circular and hexagonal patches, equation (1) can be applied for designing an HMPA. Let there be a circular patch of radius  $a$ ; the area of this patch is:

$$area_{circle} = \pi a^2 \quad (5)$$

A regular hexagon is constructed by drawing six equilateral triangles. As is known the area of an equilateral triangle of side  $s$  is given by equation (6):

$$area_{equi-triangle} = \frac{\sqrt{3}s^2}{4} \quad (6)$$

Then the area of a regular hexagon is given by equation (7):

$$area_{regul-hexagon} = \frac{3\sqrt{3}s^2}{2} \quad (7)$$

The hexagon side is determined by comparing the areas of hexagonal and circular patches as shown in equation (8):

$$\pi a_{eff}^2 = \frac{3\sqrt{3}s^2}{2} \quad (8)$$

By taking fringing into account, the hexagonal side is:

$$s = 1.0997a_{eff} \quad (9)$$

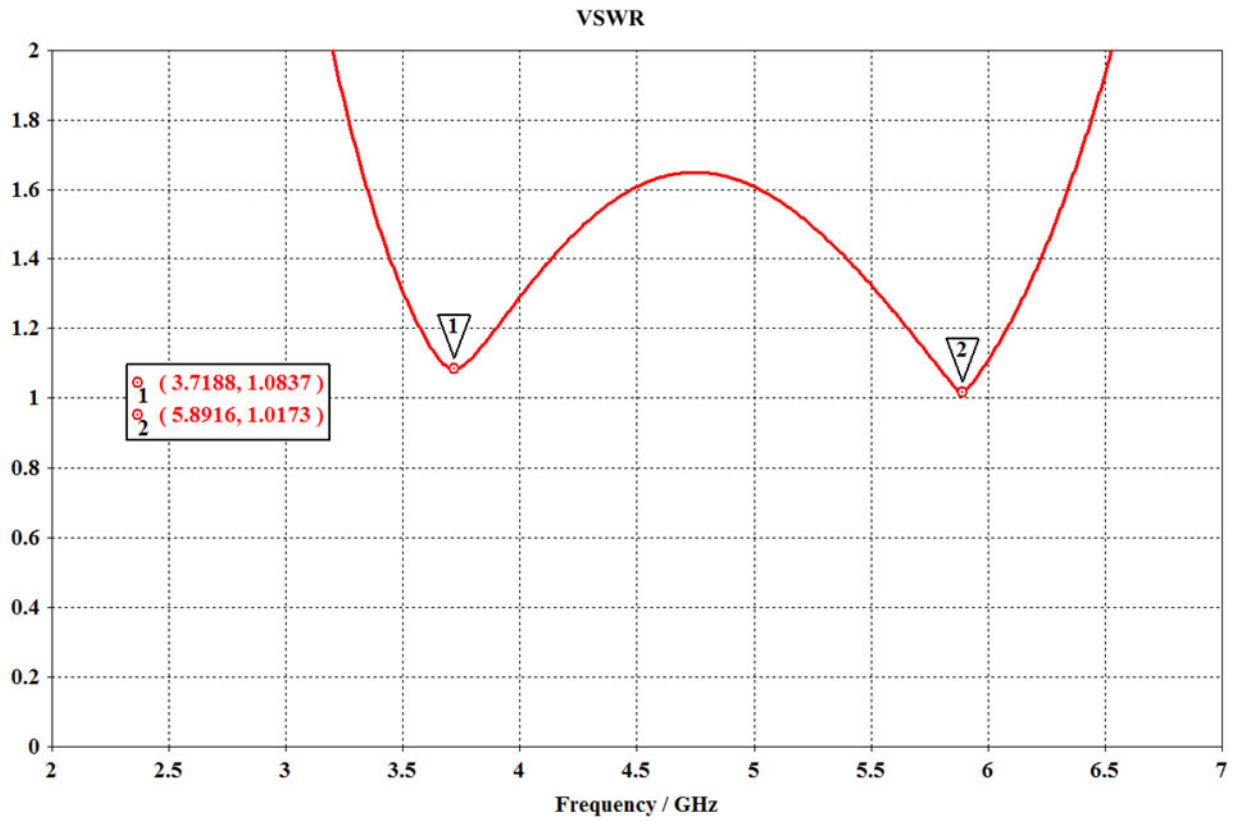


Fig. 8. VSWR of the proposed antenna.

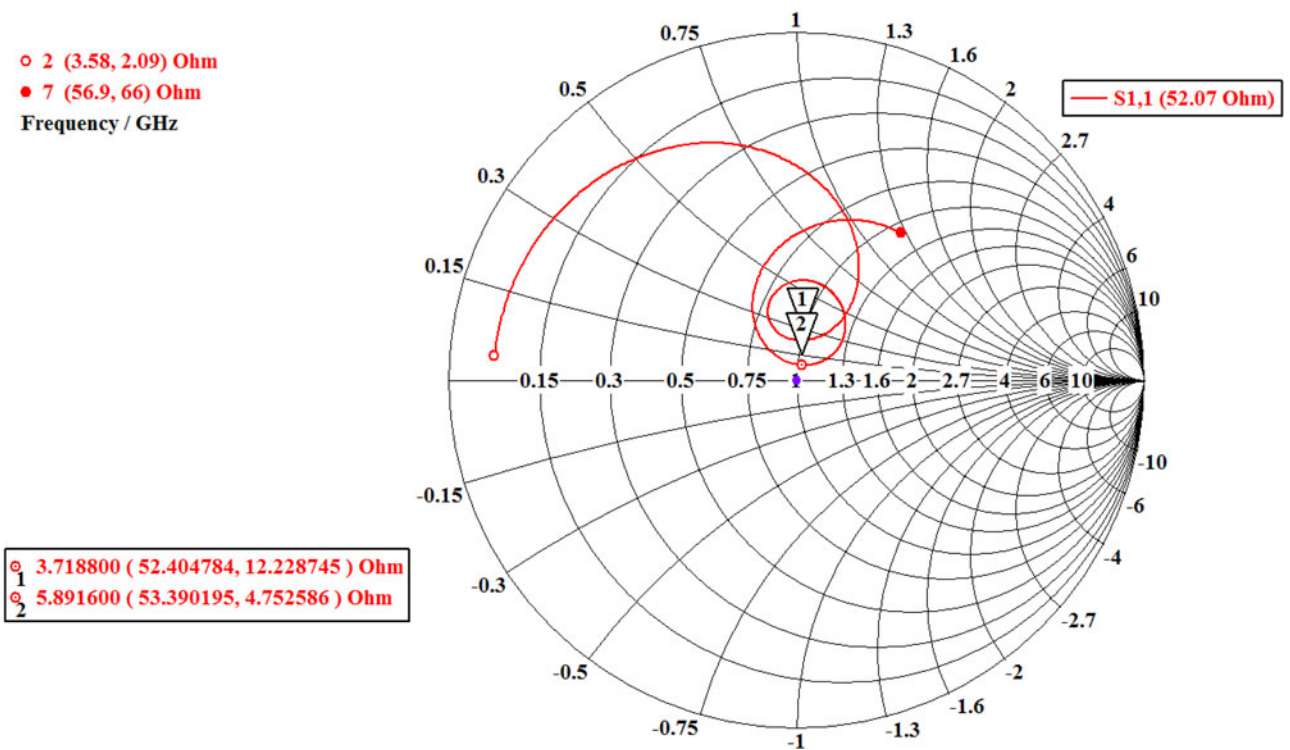


Fig. 9. Smith chart of the proposed antenna.

**Table 3.**  $S_{11}$ , VSWR, bandwidth, and gain of both configurations

	Hexagonal shape only	Hexagonal shape with Cantor fractal
Frequency (GHz)	3.77; 5.9	3.71; 5.9
VSWR	1.15; 1.32	1.08; 1.01
$S_{11}$ (dB)	-22.726; -17.46	-27.9; -41.53
Bandwidth (GHz)	3.4	3.3
Gain (dB)	2.88; 3.45	3.2; 4.15

**Cantor set fractal theory**

Cantor dust described by mathematician Georg Cantor in 1872 is probably the oldest known fractal and the easiest to create [24–26]. The construction of this structure is based on a straight line segment from which the central third is removed. The same

operation is performed on the two remaining segments, then by successive iteration on the resulting smaller and smaller segments. This shape is characterized by a number of segments tending to become infinite with an almost zero length. The number of copies of the original shape obtained from one iteration to another is equal to 2 ( $N = 2$ ) and the size of each new copy is equal to 1/3 of the original size ( $r = 1/3$ ). This geometry is described by using the iterated function system (IFS) which is represented by the following affine transformation [10]:

$$w_i \begin{bmatrix} x \\ y \end{bmatrix} = \begin{bmatrix} a_i & b_i \\ c_i & d_i \end{bmatrix} \times \begin{bmatrix} x \\ y \end{bmatrix} + \begin{bmatrix} e_i \\ f_i \end{bmatrix} \tag{10}$$

The IFS coefficients for the Cantor set are given in Table 1. In general, the fractal geometry has a very particular feature that its dimension exceeds its topological dimension, indeed there are various types of representations used for the fractal

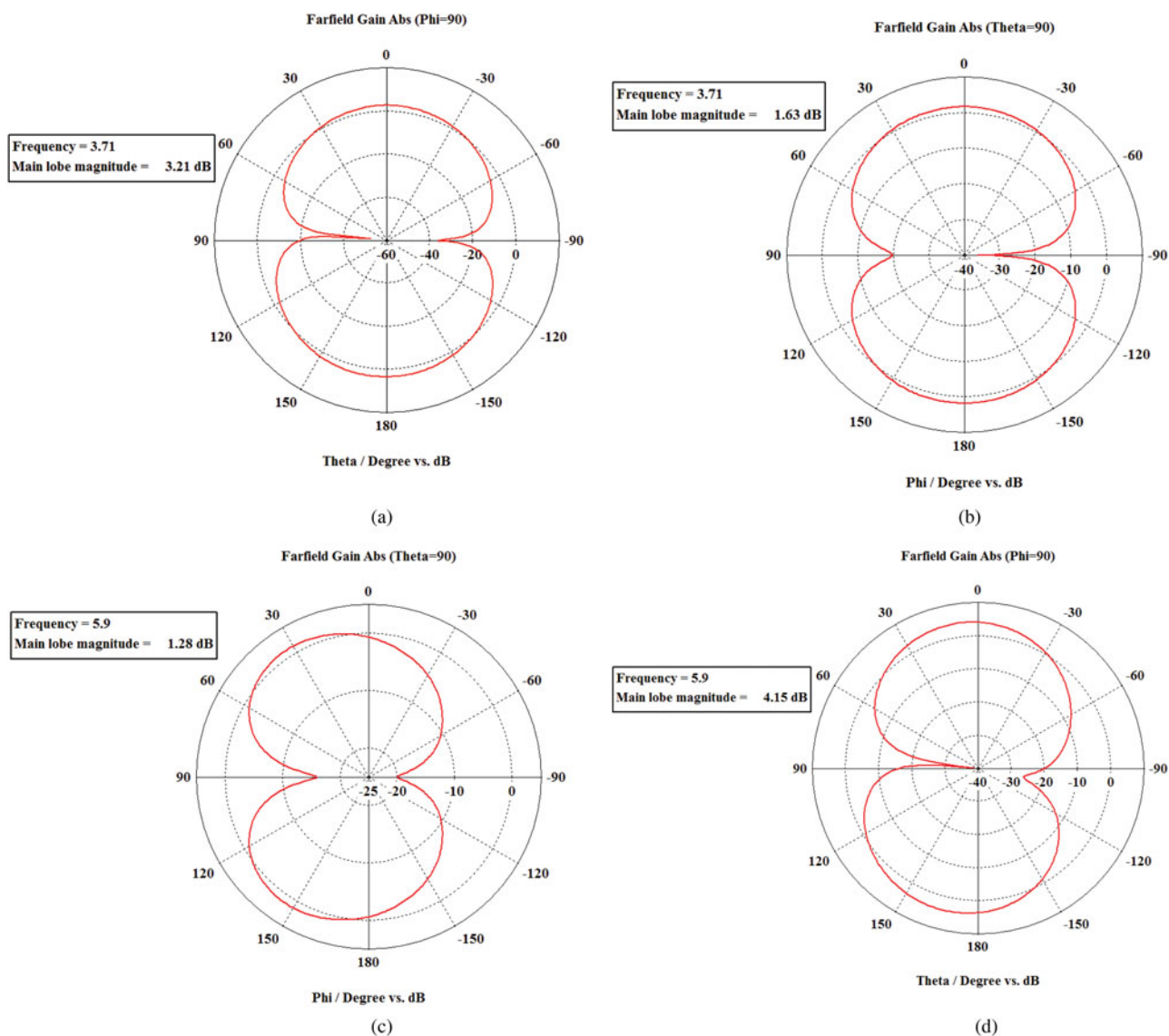


**Fig. 10.** Radiation pattern ( $E$ -plane and  $H$ -plane) at 3.71 and 5.9 GHz.

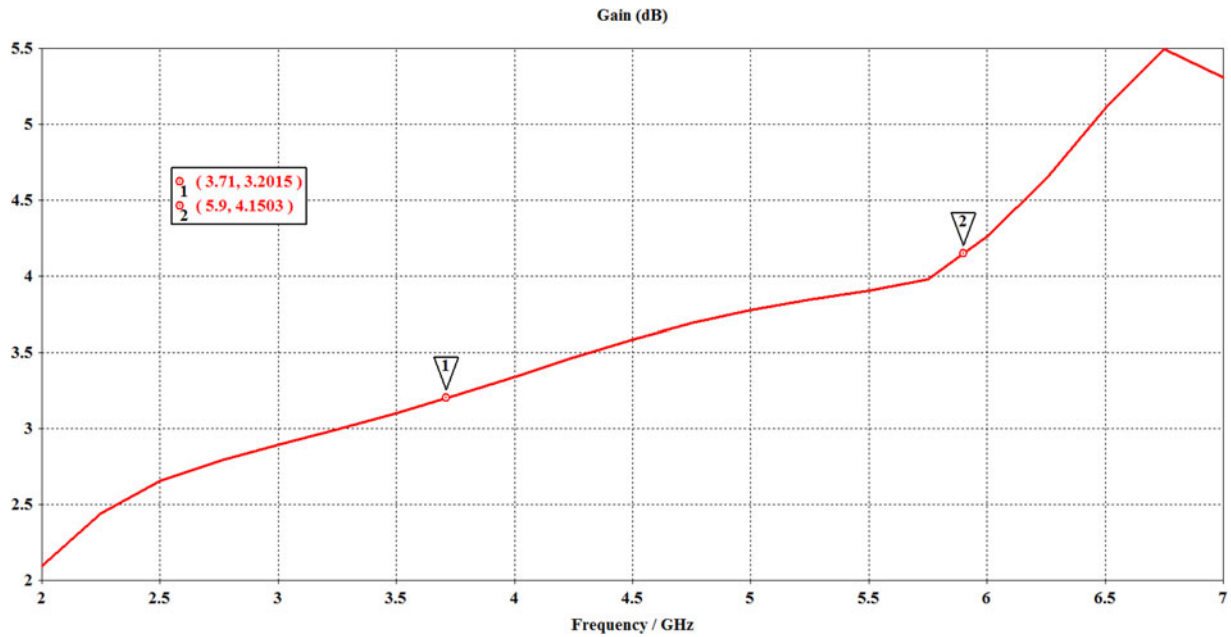


Fig. 11. Simulated gain of the proposed antenna.

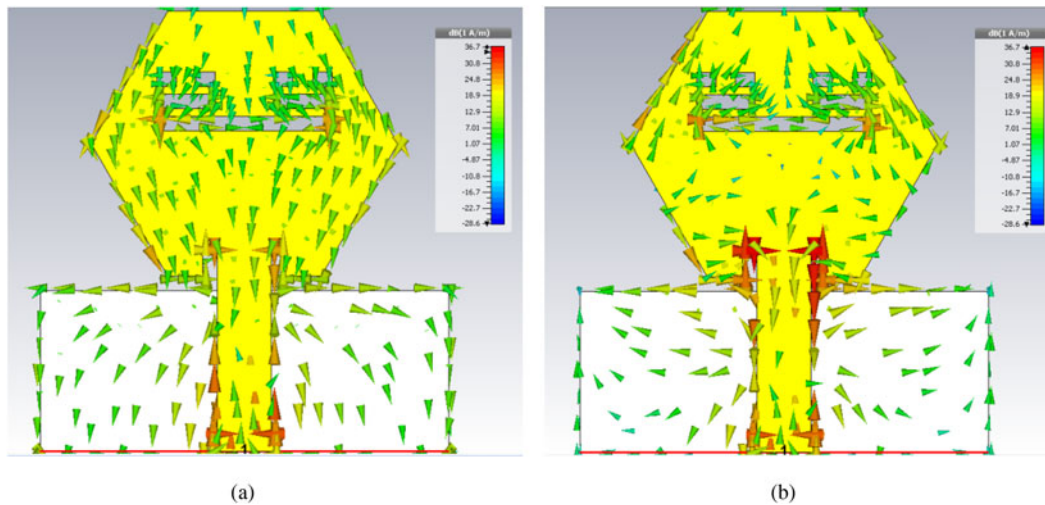


Fig. 12. Current distribution at (a) 3.71 GHz and (b) 5.9 GHz.

dimensions such as Hausdorff dimension defined as:

$$D = \frac{\ln(n)}{\ln(r)}, \tag{11}$$

where  $r$  is the scaling factor and  $N$  is the number of self-similar structure copies. The Cantor set fractal consists of  $N = 2$  congruent subsets, where each gives the original set when it is enlarged by a factor  $r = 3$ . Therefore, the fractal dimension of the Cantor set is defined as in equation (12):

$$D = \frac{\ln(2^n)}{\ln(3^n)} = \frac{\ln(2)}{\ln(3)} = 0.630929 = 0.631. \tag{12}$$

The construction of the investigated antenna is started with a simple hexagonal patch. The antenna is manufactured on an FR4 epoxy substrate with an  $\epsilon_r$  of 4.4 and a loss tangent of 0.0028. The volume of the antenna is  $L_s \times W_s \times h = 31 \times 28 \times 1.6 \text{ mm}^3$ , with a partial ground plane of  $L_g \times W_g$  at the bottom of the substrate (Fig. 1). The  $50 \Omega$  impedance is achieved by adjusting the feed line width and length (respectively  $w_f$  and  $L_f$ ), the gap ( $g$ ) notch width, and the inset distance ( $d$ ) from the radiating edge. The antenna was designed and simulated using CST Microwave Studio, which uses the finite integration technique for computation. To show the effect of inserting fractal geometry into the patch, the structure has been designed with three iterations of the Cantor set fractal geometry that has been introduced on the hexagonal patch. The side  $s$  of the hexagon shape is computed



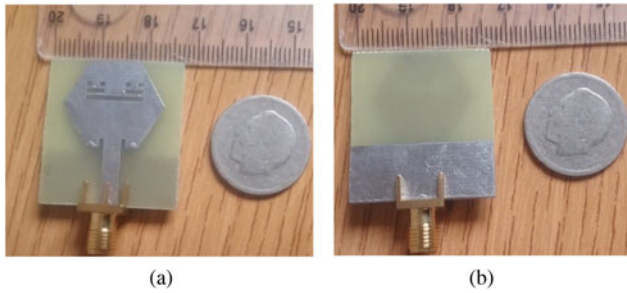


Fig. 13. Fabricated prototype of the proposed antenna: (a) front view and (b) back view.

using equation (9). At a resonant frequency, the evaluated hexagonal side  $s$  is of 21.92 mm.

Parametric study

The antenna performance is affected by several parameters such as the distance ( $d$ ) between the radiating patch and feed line, the length ( $Lg$ ) of the ground plane, the length ( $Lf$ ) and width ( $wf$ ) of the feed line, the length ( $Lc$ ) and width ( $Wc$ ) of the Cantor set slots.

As shown in Fig. 2, changing the length of the ground plane  $Lg$  not only changes the lateral dimensions of the antenna but also has a remarkable effect on the resonant characteristics of the proposed antenna. At the high  $Lg$  values, the frequency performance degrades. The optimum ground plane length is  $Lg = 11$  mm, for which the desired band frequency is obtained.

To improve the attained characteristics, the proposed antenna is simulated by keeping the length  $Lf = 12$  mm and varying the width ( $wf$ ) of the feed line. The return loss graphs of MPA along with various values of  $wf$  is shown in Fig. 3. It can be pre-meditated that the desired wideband characteristics have been exhibited with the feed line dimensions of  $Lf = 12$  mm and  $wf = 3.5$  mm. The distance ( $d$ ) between the radiation patch and

Table 4. Comparison of measurement and simulation results

-	Resonant frequency (GHz)	Bandwidth (GHz)
CST Studio Suite	3.71; 5.9	3.3 (from 3.22 to 6.5)
HFSS software	3.74; 5.91	3.16 (from 3.31 to 6.47)
Measured	3.51; 5.84	2.92 (from 3.08 to over 6)

the feed line has an important effect on the impedance matching of the antenna. From Figs 4 and 5, it can be elaborated that the desired features have been attained at the inset feed line distance of  $d = 2$  mm and a gap of  $g = 1$  mm. The Cantor fractal slots are introduced in the upper part of the hexagonal patch. A simple parametric study of the width ( $Wc$ ), the length ( $Lc$ ) of these slots, and the space between them ( $Epsc$ ) have brought us back to results depicted in Fig. 6.

It can be claimed that the Cantor slots width ( $Wc$ ) of 12 mm, length ( $Lc$ ) of 1 mm, and ( $Epsc$ ) of 0.5 mm are found to be optimum, for which the desired DSRC frequency band of 5.9 GHz is achieved.

It may be noted from Fig. 7 that the structure with Cantor fractal slots presents an improved matching and good return losses compared with the one without the fractal slots. The hexagonal-shaped structure with a Cantor fractal geometry covers the desired band exhibiting good performances.

Results and discussion

The optimized parameter dimensions of the HMPA are indexed in Table 2.

The antenna parameters such as return loss  $S_{11}$  shown in Fig. 7, VSWR in Fig. 8, the impedance in Fig. 9, and the simulated bandwidth and gain are listed in Table 3.

The minimal values of  $S_{11}$  are  $-27.9$  dB and  $-41.53$  dB at 3.71 and 5.9 GHz, respectively, which indicates a good adaptation. The efficiency of the antenna is evaluated by simulating its VSWR for

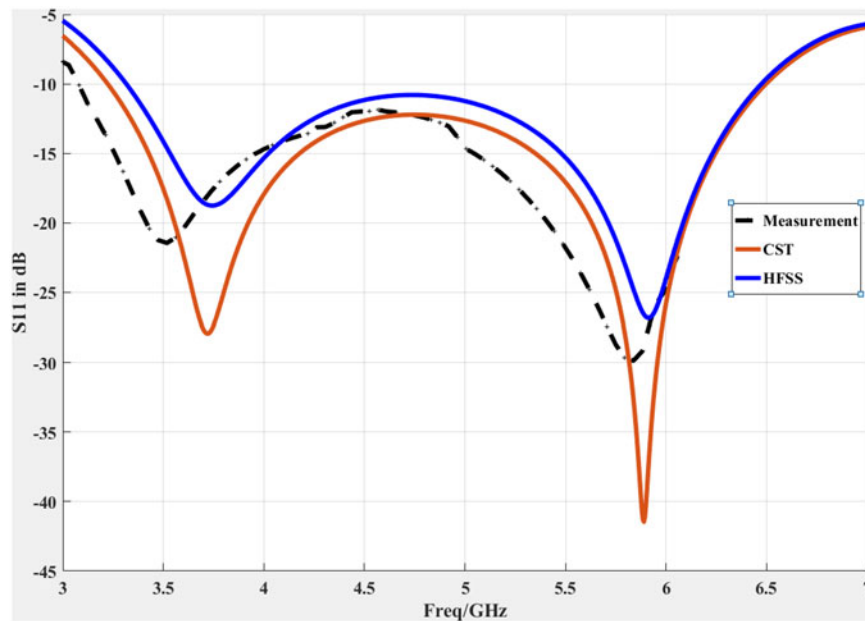
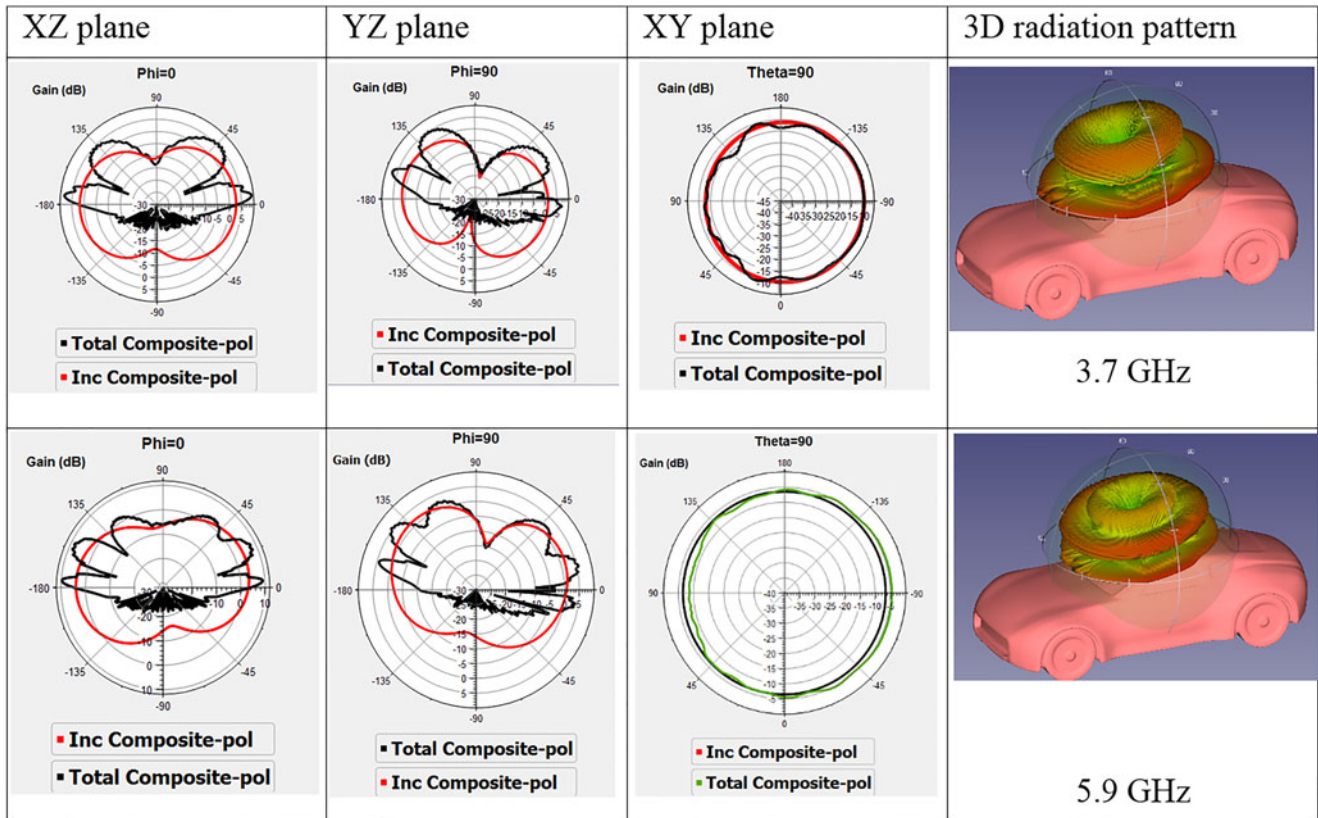


Fig. 14. Measured and simulated S-parameters of the proposed antenna.

**Table 5.** Comparison with previously published studies

Ref.	Resonant frequencies (GHz)/ $S_{11}$ (dB)	Bandwidth (MHz)	Gain (dB)	Dimensions ( $W \times L \times h$ ) mm <sup>3</sup>
Proposed	3.71/ - 27.9	3300	3.2	$31 \times 28 \times 1.6 = 1388.8$
	5.9/ - 41.53		4.15	
[26]	2.9/ - 30	650	-	$50 \times 42 \times 1.6$
	5.3/ - 24	1700		
	5.8/ - 18	850		
	8/ - 12	850		
	10/ - 12			
[24]	2.45/ - 24	1260	2.8-3.5	$50 \times 50 \times 1.6$
	5.8/ - 24	1100	3.7-4.3	
[17]	5.9/ - 57	2050	4.2	$\pi \times R^2 \times h = 8460$
[27]	1.575	100	2	$55 \times 55 \times 3.2$
	5.8	850	4/5	
[28]	2.5/ - 14	540		$21.98 \times 36.28 \times 1.6$
	5.8/ - 8	450		
[29]	1.66/ - 15	300	6	$31 \times 30 \times 1.6$
	3.48/ - 32	300	1.5	
	5.54/ - 15	1300	1.6	
[30]	1.9/ - 12	120	9	$55 \times 46 \times 1.58$
	3.7/ - 34	260	3	
	6/ - 20	330	5.3	
	7.9/ - 17	690	5.1	



**Fig. 15.** Far-field patterns of the proposed antenna mounting on front window.

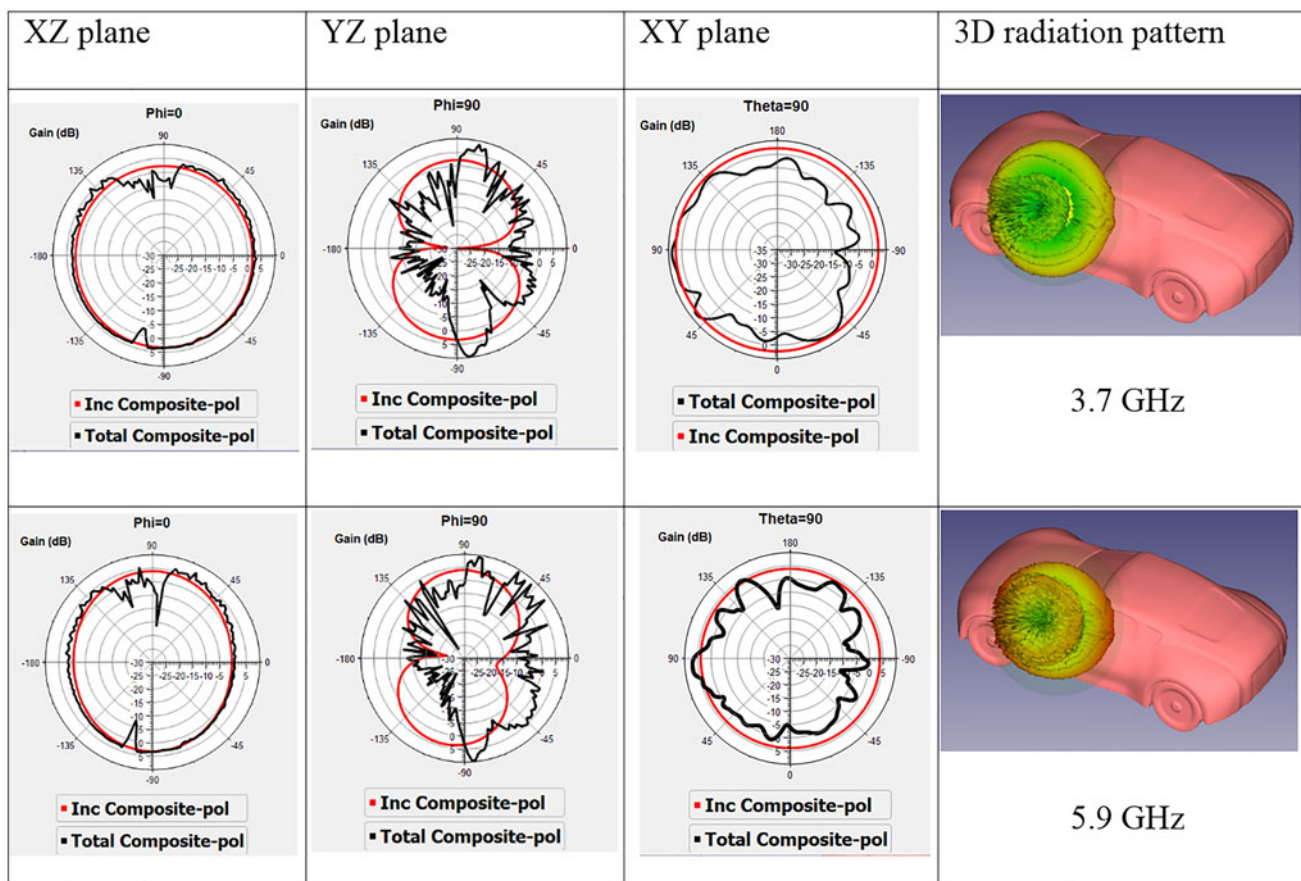


Fig. 16. Far-field patterns of the proposed antenna mounting on side mirror.

the desired frequency band. It is clear from Fig. 10 that VSWR is 1.08 at 3.71 GHz, 1.01 at 5.9 GHz, and  $<2$  across the integral bandwidth which represents a suitable efficiency of the simulated antenna.

The value of the real part of the input impedance is  $50 \Omega$  as shown in Fig. 9, which represents a null imaginary part whence the good adaptation of the antenna.

Figure 10 shows the polar radiation patterns at both resonant frequencies of 3.71 and 5.9 GHz, it is observed that the antenna has an omnidirectional behavior in both  $H$ -plane ( $\Theta = 90$ ) and  $E$ -plane ( $\Phi = 90$ ) at both resonant frequencies.

For the DSRC application, the antenna is commonly needed to hold an omnidirectional radiation pattern in the azimuth plane. From the simulated radiation patterns of the proposed HMPA at two frequencies namely 3.71 and 5.9 GHz it can be seen that the projected antenna is a good candidate for the vehicular applications. The simulated gain of the proposed antenna is illustrated in Fig. 11, which varies from 2.97 dB at the lower frequency to 5.11 dB at the upper frequency. The current distribution at the centered frequencies respectively of 3.71 and 5.9 GHz is depicted in Fig. 12. It may be claimed that the antenna principally behaves as a radiating slot formed between the hexagonal patch and the inset feed line. As displayed the current distribution at 5.9 GHz shows more concentration of the current near Cantor set fractal slots and inset feed line.

Figure 13 illustrates the fabricated model of the proposed antenna. The  $S_{11}$  of the fabricated antenna is measured using

the ANRITSU MS2026C Network Analyzer. Figure 14 shows the measured and simulated  $S$ -parameters of the proposed HMPA. It may be noted that the investigated design presents a bandwidth ( $-10$  dB) of about 3.28 GHz in simulation using the CST Studio Suite, about 3.15 GHz using HFSS software, and over than 2.92 GHz in measurement, respectively. Then it is clear that the proposed antenna displays suitable agreement in both simulation and measurements with good characteristics. A brief comparison between simulated and measured resonant frequencies and bandwidths of the simulated and manufacturing antenna is depicted in Table 4. The analysis of the results reveals that this antenna is qualified to cover many operating bands such as WLAN, WiMAX, V2X-LTE, and DSRC for vehicular communications.

Table 5 summarizes a comparison of the performance of the projected antenna with some measured antennas in previously published studies, in terms of size, resonant frequencies,  $S_{11}$  values, gain, and ( $-10$  dB) bandwidths.

#### Antenna positioning on the vehicle

The proposed antenna regards to operate among two bands for vehicular communication. It is indispensable to study the impact of the antenna placement when inserted on the vehicle platform on radiation performance and efficiency. Indeed, a CAD model of a car is taken, and three antenna positions are chosen to be tested on the roof top, side mirror, and front window of the

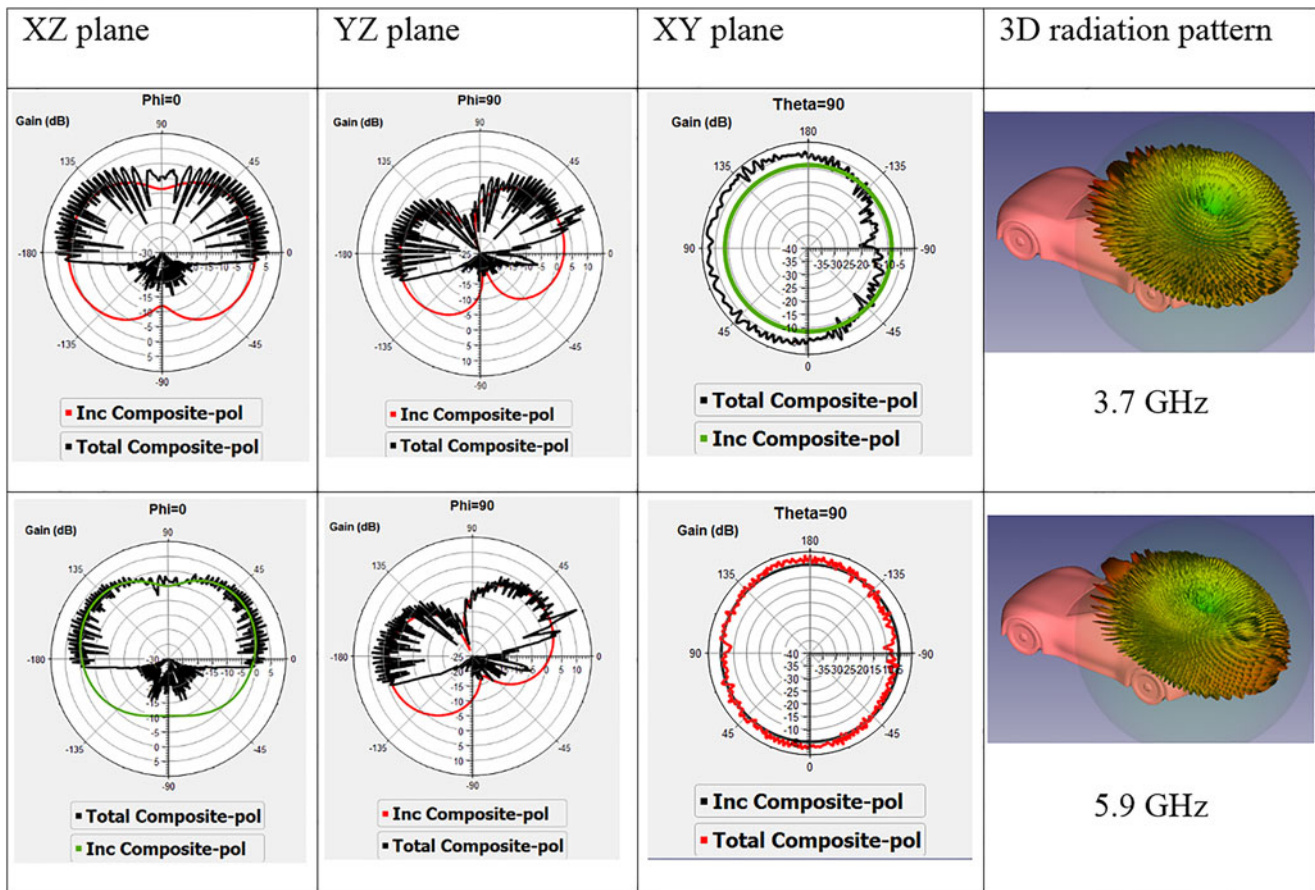


Fig. 17. Far-field patterns of the proposed antenna mounting on roof top.

vehicle. The prediction of far-field radiation characteristics of the antenna is performed employing an environment of the car body tool. Once the investigated antenna is installed at the intended locations on the car body, it will induce surface currents on the vehicle platform. These currents are then approximated by tracing high-density rays and then radiated to determine the influence of the body on the antenna radiation [20]. The simulated radiation patterns are presented in the  $XY$  ( $\Phi = 0$ ),  $YZ$  ( $\Phi = 90$ ), and  $XZ$  ( $\Theta = 90$ ) planes and are shown in Figs 15, 16, and 17, respectively. The obtained radiation patterns for the antenna at 3.7 and 5.9 GHz are slightly changed. Figure 15 depicts the radiation pattern that simulated in the windshield mounting. It can be mentioned that at 3.7 and 5.9 GHz, the obtained radiation patterns of the antenna are toward omnidirectional. The antenna in this position exhibits a good radiation pattern and less distortion which indicates a fairly good reception area. Figure 16 shows plots of the radiation patterns of the antenna installed on the side-view mirror of the vehicle at 3.7 and 5.9 GHz respectively. This antenna placement offered a more omnidirectional radiation pattern. From Fig. 17, when the antenna is positioned on the roof top of the vehicle, the direction of maximum radiation is observed in the region 30–90. The plots clearly show pattern distortion and several deep nulls, which is due to the reflections offered by the large perfectly electric conducting surface of the roof. The best placement for this antenna on the vehicle is the windshield. Even in this location, there still appears very little distortion due to the radiation pattern. It is worth to note that the back radiation exists in all the considered positions, and it is slightly

suppressed due to the penetration of the radiating field through the car body. In the  $XZ$  plane, the patterns are omnidirectional at 3.7 and 5.9 GHz DSRC band. Hence, the obtained radiation patterns are expected to use the proposed antenna in vehicular communications.

### Conclusion

An HMPA with Cantor set fractal slots on the radiating element has been designed, simulated, and measured. The antenna is designed for vehicular communication, including cellular V2X communication, DSRC communication based on the IEEE 802.11p protocol, and the antenna covers other wireless applications. To attain the desired characteristics, the effects of some geometrical parameters are analyzed. It has been noted that the projected antenna is suitable for vehicular communications including both LTE/WiMAX and V2X/DSRC. The printed antenna displays an omnidirectional radiation pattern in the horizontal plane for V2X. Reasonable results in terms of  $S_{11}$ , VSWR, and simulated gain are obtained within an effective bandwidth of 3.3 GHz from 3.22 to 6.5 GHz. The experimental and simulated results are in good agreement with a measurement bandwidth of 2.92 GHz and an omnidirectional radiation pattern in the  $H$ -plane. These results implies that the suggested HMPA with the Cantor fractal slots is appropriate for many bands of wireless communication systems: 3.7 GHz for blind spot detection for vehicles, 5.8 GHz for WLAN, 3.5 GHz for WiMAX, and 5.9 GHz for DSRC.

**Acknowledgements.** This study was supported by the Laboratory of Electrical Systems and Telecommunications, Faculty of Science and Technology, Cadi Ayyad University – Marrakech (LSET-UCAM) in coordination with the Laboratory of Computer Science, Networks, Telecommunications and Multimedia of the National High School of Technology, Hassan II University of Casablanca where the measurements have been carried out, and the National Center of Scientific and Technical Research (CNRST) Morocco.

## References

- Liang W, Li Z, Zhang H, Wang S and Bie R (2015) Vehicular ad hoc networks: architectures, research issues, methodologies, challenges, and trends. *International Journal of Distributed Sensor Networks* **11**, 745303.
- Pell BD, Sulic E, Rowe WS, Ghorbani K and John S (2011) Advancements in automotive antennas. In Chiaberge M (ed), *New Trends and Developments in Automotive System Engineering*. Rijeka, Croatia: INTECH Open Access Publisher, 2011, pp. 513–538.
- Neira EC, Carlsson J, Karlsson K and Ström EG (2015). Antennas and Propagation (EuCAP). In Neira C (ed), *Proceedings of the 9th European Conference*, Lisbon, Portugal, IEEE, 2015, pp. 1–5.
- Hu J, Chen S, Zhao L, Li Y, Fang J, Li B and Shi Y (2017) Link level performance comparison between LTE V2X and DSRC. *Journal of Communications and Information Networks* **2**, 101–112.
- Bustamante A, Inca S, Chuchon M, Adriano R and Samaniego J (2017) Design of a V2V communications antenna based on LTE technology and IEEE802.11p standard. *IEEE XXIV International Conference on Electronics, Electrical Engineering and Computing (INTERCON), 2017, IEEE Cuzco, Peru*, pp. 1–4.
- Constantinescu M, Borcoci E, Rasheed T and Hayes D (2011) An analysis of smart antenna usage for WiMAX vehicular communications. *International Conference on Mobile Lightweight Wireless Systems*, Javier Del Ser and al, Berlin, Heidelberg: Springer, pp. 248–257.
- Klemp O (2010) Performance considerations for automotive antenna equipment in vehicle-to-vehicle communications. *Proceedings of URSI International Symposium on Electromagnetic Theory*, Berlin, Germany. Piscataway, NJ, USA, IEEE, 2010, pp. 934–937.
- Bhatt S, Mankodi P, Desai A and Patel R (2017) Analysis of ultra wide-band fractal antenna designs and their applications for wireless communication: A survey. In Howon K and Dong-Chan K (eds), *2017 International Conference on Inventive Systems and Control (ICISC)*. Seoul, South Korea, IEEE, pp. 1–6.
- Palandöken M (2017) Dual broadband antenna with compact double ring radiators for IEEE 802.11 ac/b/g/n WLAN communication applications. *Turkish Journal of Electrical Engineering & Computer Sciences* **25**, 1326–1333.
- Rusu MV and Baican R (2010) Fractal antenna applications. In Minin I (ed), *Microwave and Millimeter Wave Technologies from Photonic Bandgap Devices to Antenna and Applications*. Rijeka, Croatia: IntechOpen.
- Gupta M and Mathur V (2017) Koch fractal-based hexagonal patch antenna for circular polarization. *Turkish Journal of Electrical Engineering & Computer Sciences* **25**, 4474–4485.
- Mondal T, Samanta S, Ghatak R and Bhadra Chaudhuri SR (2015) A novel tri-band hexagonal microstrip patch antenna using modified Sierpinski fractal for vehicular communication. *Progress in Electromagnetics Research* **57**, 25–34.
- Satish C (2014) *Inter-Vehicular Communication for Collision Avoidance Using Wi-Fi Direct* (PhD). Rochester Institute of Technology, New York, 2014.
- Tiwari N and Kumar S (2014) Microstrip patch antenna for 5.9 GHz dedicated short range communication system. *International Journal of Advance Electrical and Electronic Engineering* **3**, 1–4.
- Neira EC, Carlberg U, Carlsson J, Karlsson K and Ström EG (2014) Evaluation of V2X antenna performance using a multipath simulation tool. *The 8th European Conference on Antennas and Propagation (EuCAP)*. The Hague, Netherlands IEEE, pp. 2534–2538.
- Rao TR (2017) Design and performance analysis of a penta-band spiral antenna for vehicular communications. *Wireless Personal Communications* **96**, 3421–3434.
- Honggang H, Jiayu L, Daili H and Wei L (2016) Design of hexagon microstrip antenna for vehicle-to-vehicle communication. *The Journal of China Universities of Posts and Telecommunications* **23**, 69–76.
- Abishek EB, Raja AVP, Kumar KPC, Stephen AC and Raaza A (2017) Study and analysis of conformal antennas for vehicular communication applications. *ARPJ Journal of Engineering and Applied Sciences* **12**, 2428–2433.
- Hua Y, Huang L and Lu Y (2017) A compact 3-port multiband antenna for V2X communication. *IEEE International Symposium on Antennas and Propagation & USNC/URSI National Radio Science Meeting*. San Diego, California, USA, IEEE, pp. 639–640.
- Madhav BTP, Anilkumar T and Kotamraju SK (2018) Transparent and conformal wheel-shaped fractal antenna for vehicular communication applications. *AEU-International Journal of Electronics and Communications* **91**, 1–10.
- Mondal T, Maity S, Ghatak R and Chaudhuri SRB (2018) Compact circularly polarized wide-beamwidth fern-fractal-shaped microstrip antenna for vehicular communication. *IEEE Transactions on Vehicular Technology* **67**, 5126–5134.
- Usha Devi Y, Rukmini MSS and Madhav BTP (2018) A compact conformal printed dipole antenna for 5G based vehicular communication applications. *Progress in Electromagnetics Research* **85**, 191–208.
- Balanis CA (2016) *Antenna Theory: Analysis and Design*. Hoboken, New Jersey: John Wiley & Sons.
- Ali J, Abdulkareem S, Hammoodi A, Salim A, Yassen M, Rashed Hussan M and Al-Rizzo H (2016) Cantor fractal-based printed slot antenna for dual-band wireless applications. *International Journal of Microwave and Wireless Technologies* **8**, 263–270.
- Manimegalai B, Raju S and Abhaikumar V (2008) A multifractal Cantor antenna for multiband wireless applications. *IEEE Antennas and Wireless Propagation Letters* **8**, 359–362.
- Reha A, El Amri A, Benhammouch O, Said AO, El Ouadiah A and Bouchouirbat M (2017) CPW-fed slotted Cantor set fractal antenna for WiMAX and WLAN applications. *International Journal of Microwave and Wireless Technologies* **9**, 851–857.
- Hu Y-Z, Hu B-J and Zhang H-L (2017) A new compact dual-band CP antenna for GPS and DSRC applications. *Sixth Asia-Pacific Conference on Antennas and Propagation (APCAP)*, Xi'an, China, IEEE, pp. 1–3.
- Hussan MR (2016) A Cantor fractal based printed monopole antenna for dual-band wireless applications. *Engineering and Technology Journal* **34**, 1347–1359.
- Kumar M and Nath V (2018) Multiband CPW-fed circular microstrip antenna with modified Cantor fractal slot for DCS/GPS/WiMAX/WLAN/HiPERLAN2 applications. *International Conference on Wireless Communications, Signal Processing and Networking (WiSPNET)*. Chennai, IEEE, pp. 1–5.
- Singh SJ, Singh G and Bharti G (2017) Circular microstrip antenna with fractal slots for multiband applications. *Journal of The Institution of Engineers (India): Series B* **98**, 441–447.



**Fatima Ez-Zaki** received her Bachelor of Sciences in industrial computer, electronic, electrotechnical and automatic from Cadi Ayyad University, Marrakesh, Morocco, in 2015. She received her Master of Science and Technology (M.Sc. Tech. (Eng)) in electrical engineering from Cadi Ayyad University, Marrakesh, Morocco, in 2017. She is currently working toward her Ph.D. degree at the Department of Applied Physics, Electrical Systems and Telecommunications Laboratory, Cadi Ayyad University of Marrakesh, Morocco. Her research interest includes telecommunications, antennas, and vehicular communications.



**Hassan Belhrach** received his B.S. degree in electrical and electronics from Mohamed V University, Rabat, Morocco, in 1986, his M.S. degree in electronics and microelectronics from Bordeaux I University, France, in 1987, his Ph.D. degree in microelectronics and technology from Bordeaux I University, France, in 1990, and his Ph.D. degree in microelectronics and telecommunication from Cady Ayyad

University, Marrakech, Morocco, in 2001. Currently, he is a full University Professor of Analog and Digital Electronics at Royal Air Academy (Marrakech). His research areas include analysis and design packaging of very high-speed CMOS suitable for telecommunication applications.



**Abdelilah Ghammaz** received his Doctor of Electronic degree from the National Polytechnic Institute (ENSEEIH) of Toulouse, France, in 1993. In 1994, he went back to the University of Cadi Ayyad of Marrakech, Morocco. Since 2003, he has been a Professor at the Faculty of Sciences and technology, Marrakech, Morocco. His research interests include the field of electro-magnetic compatibility and antennas.